Field Decoupling for Real-Time Prospective Motion Correction Using Gradient Tones and Concurrent Field Monitoring

Maximilian Haeberlin[1], Lars Kasper[1], Christoph Barmet[2], David Otto Brunner[1], and Klaas Paul Pruessmann[1]

[1]*Institute for Biomedical Engineering, University and ETH Zurich, Zurich, Switzerland,* [2]*Skope Magnetic Resonance Technologies, Zurich, Switzerland*

Introduction: It has recently been proposed to combine NMR field probes and gradient tones to track rigid body head motion during imaging experiments[1]. This approach does not suffer from unstable marker placement and requires no line-of-sight access to the marker, a major drawback of current optical motion correction methods[3-4]. In contrast to other motion correction methods based on NMR field probes[2,6], the benefits of this approach lie in its ability to encode the position continuously without need for extra sequence elements and scan time. Additionally, it allows to concurrently monitor the encoding dynamic fields, which enables more accurate image reconstruction. A challenging problem of this approach is inductive coupling between the MR system's conductive structures that give rise to errors in the position determination based on gradient tones. In this work this problem is solved by correcting linear coupling between 0th and 1st order fields. The method is exemplified with a T_1-weighted spoiled gradient-echo (GRE) sequence.

Methods: In order to compute the coupling coefficients and to determine the accuracy and precision of the tones based position determination, three orthogonal gradient tones ($G_{x,y,z}$) are placed in the readout waveform's spectral spare band, allowing for synchronous image encoding and probe position determination (Fig. 1b). Under three such tones with frequencies ω_k, amplitudes g_k and phase offsets Φ_k, the temporal derivative of a probe phase φ at position r and time t is given by Eq. 1, where c denotes the coupling coefficient matrix, k and k' count the spatial dimensions and dynamic field indices, respectively, and c^{-1} is the coupling matrix' inverse. To determine the probe's coordinate along dimension l, the scalar product of $d\varphi/dt$ with $e^{-i\omega_l t}$ is computed, yielding a complex number (Eq. 2). For a given phase offset Φ_l, all possible coordinate values lie on a straight line through the origin in the complex plane (Fig. 2a). Coupling from other 1st order fields stretches and rotates this line and coupling from a 0th order field shifts it away from the origin. The latter is particularly manifest at coordinates close to zero where spatially linear fields vanish.

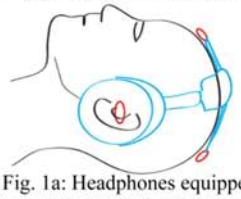

Fig. 1a: Headphones equipped with 4 ^{19}F NMR field probes.

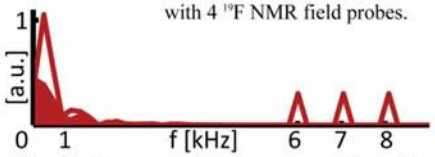

Fig. 1b: Frequency domain representation of the readout gradient waveform and the three tones.

In all experiments, a spoiled T_1-weighted GRE sequence (FOV = 0.23x0.23 m^2, resolution = 0.9x0.9x5.0 mm^3, T_{Acq} = 4.8 ms, T_R = 500 ms) was band-stop filtered to allow the insertion of 3 orthogonal gradient tones (nominal amplitude = 3.7 mT/m, frequencies = 6.0 kHz, 7.0 kHz, and 8.0 kHz, resp.). Four ^{19}F NMR field probes[5] ($T_2 \sim$ 7 ms) were mounted tetrahedrally within the gradients' linear regime inside a 3T Philips Achieva MR system.

$$\dot{\varphi}(\vec{r},t) = \gamma \sum_{k'=1}^{3} \sum_{k=1}^{3} c_{k'k} \cdot g_k \cdot r_k \cdot e^{i(\omega_k \cdot t + \Phi_k)} + c_{0k} \quad \text{Eq. 1}$$

$$\sum_{l'=1}^{3} c_{ll'}^{-1} \frac{1}{\gamma \cdot g_l} \left(\int_0^{T_{Acq}} \dot{\varphi}(\vec{r},t) \cdot e^{-i\omega_l \cdot t} dt - c_{l0} \right) = r_l \cdot e^{i\Phi_l} \quad \text{Eq. 2}$$

The 4 coupling coefficients of a gradient tone g_k were determined by taking the data from the 4 probes and solving Eq. 1 for $c_{0-3,k}$. The required reference coordinates were obtained in 3 separate scans, each employing a constant gradient. To show the improvement on probe position determination, (i) a first experiment was performed in which a volunteer was equipped with head-phones (Fig. 1a) and asked to perform rotary head motion around the magnet's main axis. The y-coordinate of a probe crossing the zero coordinate was computed with and without decoupling. (ii) In a second experiment, a volunteer performed an out-of-plane motion during an imaging experiment (T_R = 40.1 ms, 7 slices, total scan time = 72 s). A first repetition was performed without motion correction. In a second repetition, real-time prospective motion correction was applied based on probe signals. Motion correction consisted of rotating slice selection, readout and spoiler gradients, and shifting the RF excitation center frequency. In addition to motion tracking, trajectory information was extracted from the field probes and optionally used for image reconstruction. A reference trajectory was obtained by performing the same experiment in a phantom.

Results: Without decoupling, the average RMS error between measured and reference positions was (1.13 ± 0.54) mm. Decoupling reduced the error more than tenfold to $(98.1 \pm 27.3)\mu m$. The mean precision of the coordinate determination was $(89.2 \pm 31.6)\mu m$. The red dots in Fig. 2b show $r_l \cdot e^{i\cdot\Phi_l}$ for a selected probe *before* decoupling. The y-coordinate misses the origin of the complex plane, indicating residual coupling from the 0th order field. The blue dots in Fig. 2b show the same data after decoupling. 0th order contaminations have been removed completely. The effect on the y-coordinate is illustrated in Fig. 2c. Field decoupling successfully corrects erroneous sign determination for probe positions close to the center of the y-axis, where the amplitude of the coupling-induced 0th order field starts to dominate the 1st order gradient field. The rigid body translation of the head was plotted for both experiments (Figs. 3d, 3e) and amounted to $\pm$ 2x slice thickness; head rotations were small and are not shown. Motion during the experiment without motion correction causes severe image artifacts (Fig. 3a). Images from the experiment with motion correction reconstructed based on the reference trajectory still exhibit residual motion artifacts (Fig. 3b), which is due to motion between the position update (calculated in the preceding readout) and the end of the current readout. The same data reconstructed with the concurrently monitored readout trajectory are free of motion artifacts (Fig. 3c).

Conclusions: The successful implementation of 0th and 1st order field decoupling is demonstrated. It improves the accuracy of probe positioning to below 100 μm and the resulting precision is 89 μm. Concurrent field monitoring data is readily available from the same data and captures in-plane motion in the form of resulting trajectory alterations for more accurate image reconstruction.

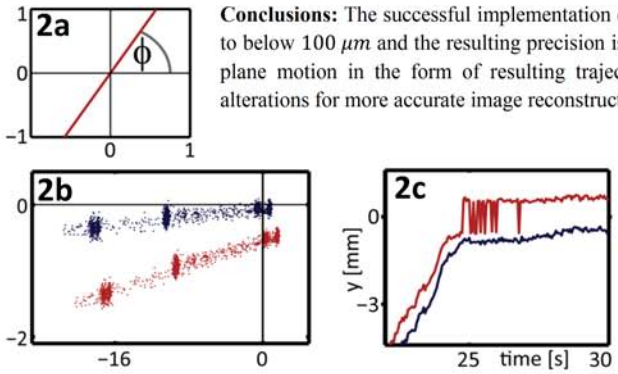

Fig. 2: 2a): For a given phase Φ, all measured positions lie on a radial line in the complex plane. 2b): measured complex coordinates of a probe in motion, before decoupling (red) and after decoupling (blue). 2c): y-coordinates of the same probe illustrating how erroneous sign determination close to zero (red) is corrected by decoupling (blue).

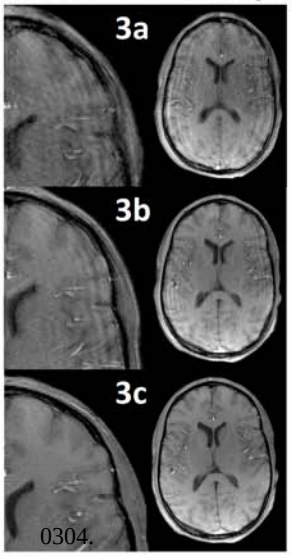

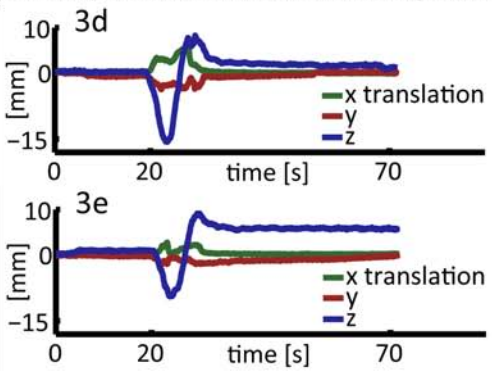

Fig. 3: Images from a multi-slice GRE acquisition are shown, acquired in the presence of motion. 3a: without motion correction. 3b: With motion correction but reconstructed with a reference trajectory. 3c: Concurrent field monitoring successfully removes these artifacts. Motion for the uncorrected and corrected images is plotted in 3d, and 3e, respectively.

References: **[1]** Haeberlin et al. Procs. ISMRM, 2012, #595. **[2]** Ooi et al. MRM 62:943–954. **[3]** Zaitsev et al. Neuroimage 31:1038–1050. **[4]** Aksoy et al. MRM 59:1138–1150. **[5]** Barmet et al. Procs. ISMRM, 2010, #216. **[6]** Krueger et al. Procs ISMRM 2006, #3196.